JACS
JOURNAL OF THE AMERICAN CHEMICAL SOCIETY
Article
Cite This: J. Am. Chem. Soc. 2018, 140, 775−782
pubs.acs.org/JACS

Entropy-Driven High Reactivity of Formaldehyde in Nucleophilic Attack by Enolates on Oxide Surfaces

Shuai Wang*,†,‡ and Enrique Iglesia*,‡

†State Key Laboratory for Physical Chemistry of Solid Surfaces, Collaborative Innovation Center of Chemistry for Energy Materials, and National Engineering Laboratory for Green Chemical Productions of Alcohols-Ethers-Esters, College of Chemistry and Chemical Engineering, Xiamen University, Xiamen 361005, China

‡Department of Chemical and Biomolecular Engineering, University of California, Berkeley, California 94720, United States

Supporting Information

ABSTRACT: CH_3OH dehydrogenation on a metal function occurs in tandem with C−C coupling of HCHO with enolates derived from alkanals or alkanones on acid−base pairs at anatase TiO_2 surfaces with very high specificity for nucleophilic attack by enolates on HCHO over larger carbonyl molecules. The measured rate constants for enolate coupling with HCHO are >10^3-fold larger than for its coupling with acetone. Free energies derived from theoretical treatments of reactions between C_2−C_4 bound enolates and carbonyls show that such specificity for nucleophilic attack on HCHO reflects smaller entropy losses upon formation of the transition state (TS), instead of enthalpic effects caused by weaker steric effects or the stronger electrophilic character of HCHO compared with larger carbonyls. The easier steric access and higher electrophilicity of the carbonyl C atom of HCHO in C−C coupling with enolates are compensated by a later TS and by stronger van der Waals contacts for the corresponding reactions of the larger carbonyls. The preeminence of entropic effects over enthalpic stabilization reflects the greater structural organization imposed by surfaces on TS structures compared with similar reactions and structures in gaseous or liquid media. Such organization imposes significant entropic penalties that become least consequential for smaller electrophiles, thus enabling highly selective routes for sequential addition of C_1 groups at nucleophilic C atoms in co-reactants using HCHO, whether added or formed in situ from CH_3OH, as the monomer source. Such entropy-driven specificity is therefore a unique and unrecognized characteristic of reactions catalyzed by surfaces.

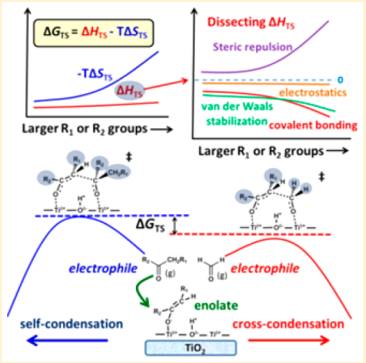

1. INTRODUCTION

Formaldehyde (HCHO) is much more reactive than other alkanals or alkanones in C−C coupling reactions with nucleophiles, such as enolates in aldol condensation[1−4] or alkenes in Prins condensation,[5,6] making it a monomer of choice in backbone lengthening strategies.[7,8] Weaker steric hindrance at C═O centers[9] and the more electrophilic character of the carbonyl C atom in HCHO[10] are often invoked in order to account for this high reactivity, but without explicit experimental or theoretical treatments of kinetic constants or of the enthalpy and entropy components of the relevant activation free energy barriers.

Lewis acid−base pairs (metal−oxygen linkages) of moderate strength on TiO_2 and ZrO_2 show unique reactivity in surface-catalyzed aldol condensations.[9,11−14] These reactions are limited by enolate formation steps that cleave α-C−H bonds in carbonyl reactants[9,11] and involve subsequent fast nucleophilic attack on co-adsorbed reactants by enolates and H_2O elimination to form α,β-unsaturated carbonyls, as well as their hydrogenated products (alkanals, alkanones, and alkanols) when a metal function (Cu,[11] Pt,[15] Ag used here) and H_2 are also present (Scheme 1). HCHO is unable to form enolates because it lacks α-C−H bonds, but it is highly reactive as the electrophile in C−C bond formation with α-C atoms in bound enolates.[1−4]

Scheme 1. Self Condensation and Cross Condensation Pathways for C_n Carbonyl Compounds (n = Number of C-Atoms) and HCHO on Anatase TiO_2 (with Ag/SiO_2 Co-Catalysts and Added H_2)

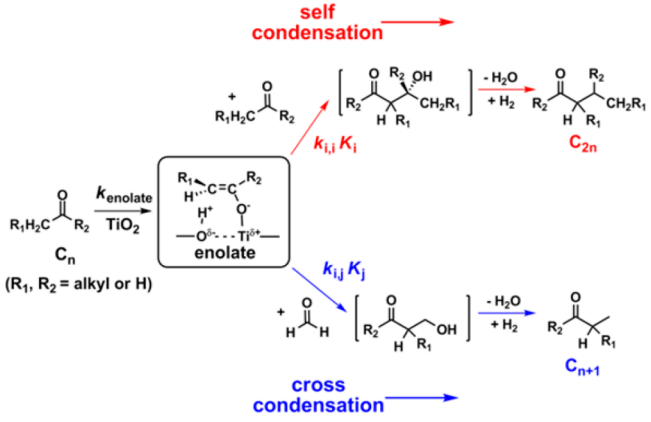

Received: November 5, 2017
Published: January 3, 2018

DOI: 10.1021/jacs.7b11749
J. Am. Chem. Soc. 2018, 140, 775−782

Additionally, HCHO can be formed in situ via dehydrogenation of CH_3OH on metal catalysts (Cu,[16] Ag[17]) present as mixtures with TiO_2 or ZrO_2, thus enabling the use of CH_3OH here as a C_1 monomer in carbon chain lengthening reactions that is less costly and easier-to-handle than HCHO.

Here, we combine kinetic and theoretical methods to examine the C−C coupling reactions of C_2−C_4 enolates with HCHO and with larger carbonyl reactants on anatase TiO_2 (TiO_2(a)) using Ag/SiO_2 as co-catalysts in experiments in order to convert CH_3OH to HCHO. The effects of alkyl substituents in carbonyls on C−C bond formation rates and on the enthalpy and entropy components of activation free energy barriers for self-condensation and C−C coupling with HCHO (Scheme 1) are assessed using state-of-the-art theoretical treatments, with acetone-HCHO reactions used as the experimental benchmark. The uniquely high reactivity of HCHO (relative to larger alkanals or alkanones) with a given enolate does not reflect a greater enthalpic stabilization of transition states (TS), typically expected for HCHO, which is the stronger electrophile and has a sterically less hindered C atom; these expected enthalpic effects are offset by stronger van der Waals and covalent stabilization of the larger carbonyl molecules by the enolates at the bimolecular C−C coupling TS. They reflect instead the much smaller entropy loss upon formation of the TS with the smaller electrophiles and the preeminent role of entropy on activation free energies at the relatively high reaction temperatures required for these reactions on oxide surfaces. These entropic effects become more preeminent at surfaces which impose a greater degree of organization at TS than homogeneous gaseous or liquid media.

2. EXPERIMENTAL METHODS

2.1. Catalyst Synthesis and Characterization. Ag/SiO_2 co-catalysts (ca. 20% wt. Ag) were prepared using homogeneous deposition−precipitation methods. $AgNO_3$ (≥99.5%, Sigma-Aldrich; 5 mmol) and urea (99%, Aldrich; 25 mmol) were dissolved in 50 cm^3 deionized water at ambient temperature. Fumed SiO_2 (Cab-O-Sil, Sigma-Aldrich; 395 $m^2\ g^{-1}$; 2.0 g) was then added into this solution, and the pH value of the suspension was adjusted to 2−3 using HNO_3 solutions (0.5 mmol cm^{-3}; 99%, Sigma-Aldrich). This suspension was heated to 353 K (at 0.167 K s^{-1}) and held for 20 h under stirring (12 Hz). The powders were filtered and washed with deionized water until the filtrate gave a pH value of 6−7 and then treated in ambient stagnant air at 383 K for 24 h and in flowing dry air (1.67 $cm^3\ g^{-1}\ s^{-1}$, Praxair) at 1073 K (at 0.033 K s^{-1}) for 2 h. These samples were finally treated in flowing 10% H_2/He (5.56 $cm^3\ g^{-1}\ s^{-1}$, Praxair) by heating to 803 K (at 0.033 K s^{-1}; held for 2 h) and then in flowing 1% O_2/He mixtures (0.83 $cm^3\ g^{-1}\ s^{-1}$, Praxair) at ambient temperature for 1 h to passivate the samples before exposure to ambient air. Cu/SiO_2 co-catalysts (ca. 20% wt. Cu) were also prepared using homogeneous deposition−precipitation methods that are described elsewhere in detail.[11]

These Ag/SiO_2 and Cu/SiO_2 samples were characterized by powder X-ray diffraction (XRD) (Cu Kα radiation, λ = 0.15418 nm, 40 kV, 40 mA, Bruker D8 Advance). The mean crystallite size of metal particles in these samples was determined from the breadth of their most intense (111) reflections in XRD diffractograms (2θ: 38.1° for Ag; 43.3° for Cu) using the Scherrer equation.[18] The mean Ag crystallite size of the Ag/SiO_2 catalysts was 15.5 nm, and that for the Cu particles in the Cu/SiO_2 catalysts was 7.9 nm.

Anatase TiO_2 (TiO_2(a), 99.7%, 240 $m^2\ g^{-1}$, Alfa Aesar) was used here as the condensation catalyst. It was treated at 673 K (0.167 K s^{-1}) for 3 h in flowing dry air (1.67 $cm^3\ g^{-1}\ s^{-1}$, 99.999%, Praxair) before use. The crystalline phase of TiO_2(a) was confirmed by XRD.

2.2. Rates of Acetone-HCHO Condensation Reactions. TiO_2(a) and Ag/SiO_2 (or Cu/SiO_2) co-catalysts were mixed together using a mortar and pestle with a mass ratio that ranged from 1/2−1/8. Aggregates of these mixtures (125−180 μm), obtained via pressing, crushing, and sieving, were loaded into a quartz tubular flow reactor (1.0 cm I.D.), treated in flowing 10% H_2/He (5.56 $cm^3\ g^{-1}\ s^{-1}$, 99.999%, Praxair) at 803 K (0.0833 K s^{-1} from ambient temperature) for 2 h, and then cooled to desired reaction temperature (723−773 K). Liquid acetone (99.9%, Fisher Scientific) and methanol (HCHO precursor, 99.9%, Fisher Scientific) were introduced into the reactor via vaporizing into H_2 (99.999%, Praxair) and He (99.999%, Praxair) flows, and the liquid and gas flow rates were metered via syringe pumps (Cole Parmer, 74900 series) and electronic mass flow controllers (Porter, Inc.), respectively. All transfer lines were kept above 430 K in order to avoid reactant or product condensation.

The concentrations of the effluent components were measured by gas chromatography (Agilent 6890) using a capillary column (Agilent, HP-1, methyl silicone, 50 m, 0.32 mm I.D. × 1.05 um) connected to a flame ionization detector and also a packed column (Porapak-Q, 4.8 m, 80−100 mesh) connected to a thermal conductivity detector. Conversions and selectivities were reported on a carbon basis. Reaction rates were measured periodically at a reference condition (1.0 kPa acetone, 5.0 kPa methanol, 10 kPa H_2, 773 K) to correct rates for some slow deactivation detected at the reaction conditions used in this study.

2.3. Computational Methods. $Ti_5O_{19}H_{18}$ clusters (Scheme 2) were extracted from TiO_2(a) (101) surfaces as described elsewhere.[11]

Scheme 2. $Ti_5O_{19}H_{18}$ Cluster Model Built Based on the Anatase TiO_2 (101) Surface Structure

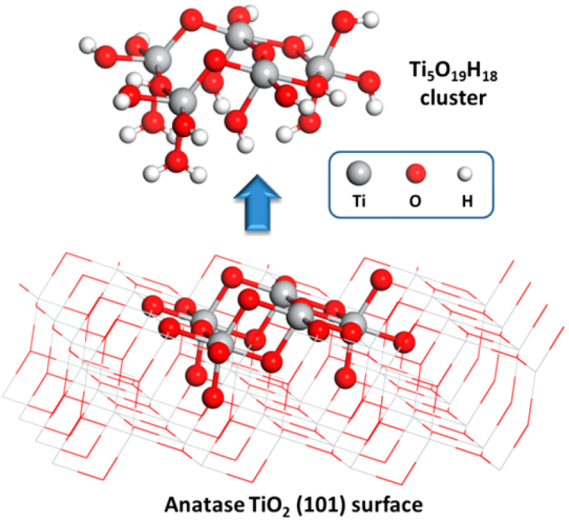

These $Ti_5O_{19}H_{18}$ clusters have been shown to represent adequate models in assessing the elementary steps and their kinetic relevance in aldol condensations on TiO_2(a).[9,11] Geometry optimizations of reactants, products, and TS involved in enolate-carbonyl C−C coupling reactions on $Ti_5O_{19}H_{18}$ clusters were carried out using the Berny geometry algorithm[19] as implemented in the Gaussian 09 program.[20] During optimizations, the five Ti atoms and the three internal O atoms in $Ti_5O_{19}H_{18}$ clusters were allowed to relax, while all remaining atoms were held fixed in order to preserve the structure of the extended parent anatase surfaces. All calculations were carried out at the hybrid B3LYP functional level of theory[21,22] with the Gaussian-type 6-311G(d,p) basis set for the C, O, and H atoms[23,24] and the effective core potential LANL2DZ basis set for the Ti atoms.[25] Wave functions were converged to 10^{-8} Ha with an ultrafine grid of 99,590 points for the numerical integration; structures were optimized until the root-mean-square force was <1.5 × 10^{-5} Ha $Bohr^{-1}$. The van der Waals contributions to electronic energies were calculated for all structures using Grimme's D3BJ dispersion correction[26] in each step of the geometry optimization. The overestimation of binding energies brought forth by the basis-function overlaps when finite basis sets are used, known as the basis set superposition error, was eliminated using the counterpoise correction

DOI: 10.1021/jacs.7b11749
J. Am. Chem. Soc. 2018, 140, 775−782

method.[27,28] These optimized structures were further examined by frequency calculations at the same computational level.

Zero-point energies and thermal corrections used to calculate the enthalpy and entropy of each structure were determined using DFT-derived frequencies with the rigid rotor harmonic oscillator (RRHO) approximation.[29] A factor of 0.9682 was used to scale these frequencies to compensate anharmonicity effects excluded in RRHO treatments.[30] In addition, the vibrational entropies corresponding to the low-frequency modes of weakly bound adsorbates (<100 cm^{-1}; listed in Table S1, Supporting Information (SI)) were calculated using a free-rotor model, as proposed by Grimme,[31,32] because of the significant errors in the vibrational entropies derived from RRHO treatments of such modes.[33] The charges of each atom in all reactants, products, and TS structures were calculated using the natural bond orbital (NBO) analysis[34] that provided the most likely Lewis electronic structure for each molecule or coordination complex, and the properties of chemical bonds in these structures were analyzed using the Wiberg bond indices.[35,36]

3. RESULTS AND DISCUSSION

3.1. Formation of HCHO via CH_3OH Dehydrogenation on Cu/SiO_2 and Ag/SiO_2 Catalysts. Use of CH_3OH as a precursor to HCHO is favorable over direct introduction of HCHO because of the chemical instability, volatility, and toxicity of HCHO reactants and the fact that HCHO is available only as dilute aqueous solutions (~60% H_2O by volume). HCHO can form in situ from CH_3OH on a dehydrogenation function (e.g., Cu[16] and Ag[17]) and then be scavenged by condensation reactions with C_{2+} alkanals/alkanones in the presence of an acid–base function (e.g., anatase TiO_2 (TiO_2(a)), as shown below, thus minimizing HCHO decomposition to CO and H_2. These tandem dehydrogenation–condensation processes would also lead to a novel and practical approach to using methanol as a C_1 growth monomer with the formation of specific skeletal structures unavailable from methanol homologation catalyzed by Brønsted acids.[6]

Cu dehydrogenates CH_3OH to HCHO,[16] but forms methyl formate as the predominant product (Figure S1, SI). Ag/SiO_2, in contrast, gives HCHO selectivities above 60% (5% CH_3OH conversion; 773 K, Figure 1), leading to higher prevalent HCHO pressures in these tandem dehydrogenation–condensation processes. Therefore, Ag/SiO_2 is used in this study as the dehydrogenation co-catalyst with TiO_2(a) in effecting the cross condensation of acetone-HCHO mixtures, in which CH_3OH was used as the C_1 monomer source to form HCHO in situ.

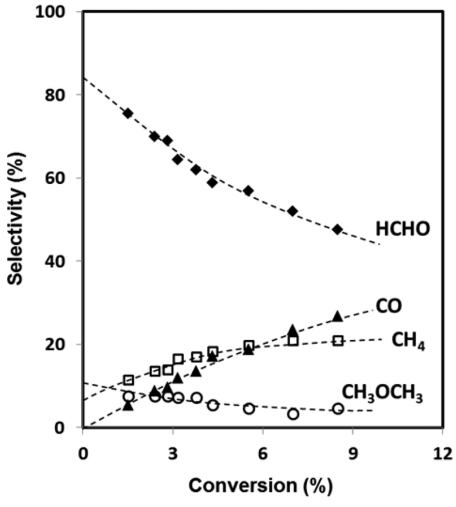

Figure 1. CH_3OH reaction selectivity on Ag/SiO_2 as a function of CH_3OH conversion (varied through changes in reactor residence time; 20% wt. Ag/SiO_2, 773 K, 5 kPa methanol, 10 kPa H_2). Dashed lines indicate trends.

3.2. Rates and Selectivities of Acetone-HCHO Condensations on Mixtures of Anatase TiO_2 and Ag/SiO_2 Catalysts. The products formed in acetone-HCHO condensation depend on the coupling rates of acetone-derived propen-2-olates with either acetone (to form 4-hydroxy-4-methyl-pentan-2-one; self-condensation) or HCHO (to form 4-hydroxy-butan-2-one; cross-condensation) on TiO_2(a). These coupling steps lead to the formation of aldols that subsequently dehydrate and hydrogenate to form methyl isobutyl ketone (C_{3+3}) and butan-2-one (C_{3+1}), respectively (Scheme 3). These larger alkanone products can also react further with acetone or HCHO, leading to primary product selectivities that ultimately decrease with increasing residence time. For instance, secondary cross-condensations between butan-2-one and HCHO produced pentan-3-one ($C_{3+1\times2}$), 3-methylbutan-2-one ($C_{3+1\times2}$), and 2-methylpentan-3-one ($C_{3+1\times3}$) (Scheme 3). The selectivity to the primary butan-2-one product decreased from 99% to 83% as the acetone conversion increased from 1% to 38% (773 K, 1 kPa acetone, 5 kPa methanol, 10 kPa H_2), while the selectivities to all secondary cross-condensation products increased (Figure 2). The selectivity to methyl isobutyl ketone (C_{3+3}) remained nearly constant at 1% throughout this acetone conversion range (Figure 2), indicating methyl isobutyl ketone is less reactive than butan-2-one in subsequent coupling reactions with HCHO.

Scheme 3. Reaction Pathways of Acetone-HCHO Condensations on Physical Mixtures of Anatase TiO_2 and Ag/SiO_2

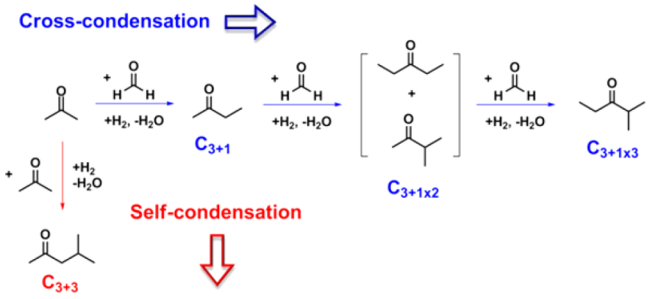

The combined rates of self-condensation (r_{self}) and cross-condensation (r_{cross}) increased linearly with acetone pressure, but did not depend on the HCHO pressure, set in these experiments by the CH_3OH dehydrogenation function (Figure 3). These data indicate that condensation rates are limited by α-C–H activation steps that form propen-2-olates from acetone on essentially bare TiO_2(a) surfaces.[11] HCHO (or CH_3OH) did not influence enolate formation rates, because of their low prevalent coverages at Ti–O site pairs. Propen-2-olates react with either acetone or HCHO to form C_6 or C_4 alkanones via competitive reactions that cause r_{self} to increase more strongly with acetone pressure than r_{cross}; at all conditions, cross-condensation events account for most of the products formed from these enolates (Figure 3a). Faster scavenging of propen-2-olates at higher HCHO pressures renders them unavailable for self-condensation, leading to r_{self} values that consequently decrease as the HCHO pressure increases (Figure 3b).

The r_{cross}/r_{self} ratios increased linearly with HCHO/acetone ratios and were much larger than unity at all conditions and even

DOI: 10.1021/jacs.7b11749
J. Am. Chem. Soc. 2018, 140, 775–782

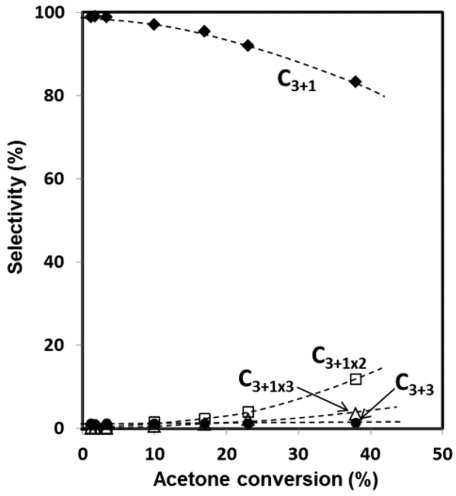

Figure 2. Selectivity of acetone-HCHO condensations as a function of acetone conversion (varied through changes in reactor residence time; TiO_2(a); 20% wt. Ag/SiO_2; 1:8 mass ratio; 773 K, 1 kPa acetone, 5 kPa methanol, 10 kPa H_2). C_{3+x} (x = 1−3) represents the respective condensation product using the nomenclature in Scheme 3. Dashed lines indicate trends.

at very low HCHO/acetone ratios (Figure 4). The slope of the data in Figure 4 reflects the ratio of rate constants for nucleophilic attack at HCHO and acetone by the bound propen-2-olates; this ratio is 1110 ± 40 (773 K), consistent with the high reactivity of HCHO relative to acetone. Heuristic constructs would typically assign such high reactivity to the less crowded nature[9] and the more electrophilic character[10] of the C atom in HCHO compared with the carbonyl C atom in larger alkanals or alkanones. Kinetic data and DFT-derived free energies are used here to provide these heuristic descriptions with a more rigorous mechanistic basis and to show that entropic effects, instead of the enthalpic considerations implicit in sterics and electrophilicity, make HCHO the preferred electrophile in nucleophilic attack by enolates on catalytic surfaces that impose a level of organization at TS absent in reactions occurring in homogeneous gaseous or liquid media.[10]

3.3. Kinetic Assessment of the Reactivity of Acetone and HCHO in Nucleophilic Attack by Enolates on TiO_2 Surfaces. Aldol condensation on TiO_2 involves C−C coupling of bound enolates, formed in rate-limiting steps, with carbonyl molecules bound weakly at vicinal Lewis acid centers (Scheme 4).[9,11] The rate of C−C bond formation between a bound enolate (EN_i*), derived from reactant i, with a carbonyl C atom in species j ($r_{i,j}$) is given by

$$r_{i,j} = k_{i,j}K_j(\mathrm{EN}_i^*)(*)P_j/(L) \quad (1)$$

where (*) is the number of unoccupied Ti−O site pairs, (L) is the total number of such pairs at oxide surfaces, P_j and K_j are the respective pressure and adsorption constant of species j, and $k_{i,j}$ is the rate constant for EN_i*-j coupling. For each i-derived enolate, the rate ratio for self ($j = i$) to cross ($j \neq i$) C−C coupling is then given by

$$\frac{r_{i,j}}{r_{i,i}} = \left(\frac{k_{i,j}K_j}{k_{i,i}K_i}\right)\cdot\left(\frac{P_j}{P_i}\right) \quad (2)$$

Eqs 1 and 2 provide general kinetic descriptions for competitive reactions of enolates with carbonyl molecules at Lewis acid−base site pairs prevalent on oxide surfaces and specifically on

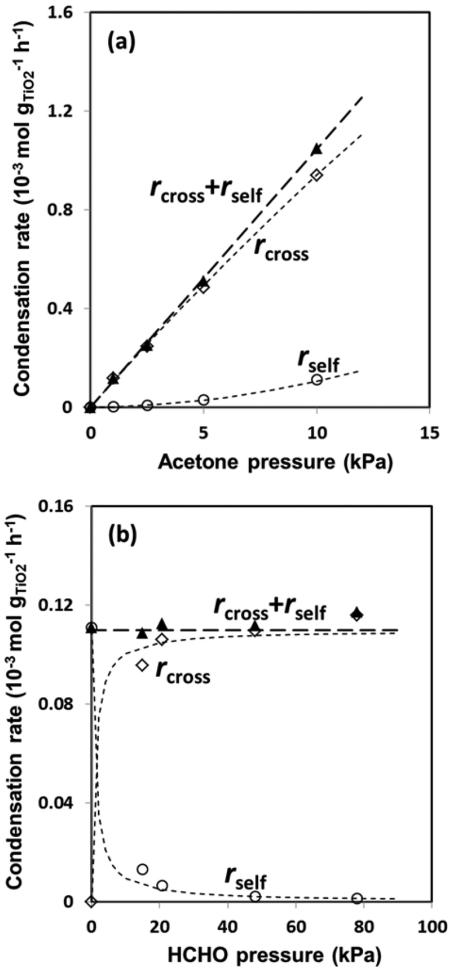

Figure 3. Self-condensation (r_{self}, ○) and cross-condensation (r_{coss}, ◇) rates of acetone-HCHO reactions and their sums (▲) as a function of (a) acetone and (b) HCHO pressures (TiO_2(a); 20% wt. Ag/SiO_2; 1:8 mass ratio; 773 K, 10 kPa H_2, 0−10 kPa acetone, 5 kPa methanol for (a); 1 kPa acetone and 0−10 kPa methanol for (b); <5% acetone conversions; HCHO pressures measured in effluent stream). Dashed lines are regression fits to the function forms of eqs S1−S3 in the SI.

TiO_2(a) and monoclinic ZrO_2 systems[9] that are particularly proficient catalysts for aldol condensations.

The slope in Figure 4 gives the $k_{i,j}K_j/k_{i,i}K_i$ ratio when i is acetone and j is HCHO. This ratio reflects the magnitude of $\Delta G^{TS}_{i,j-i,i}$, the difference between the free energy barriers to form a C−C bond between propen-2-olate and acetone ($\Delta G^{TS}_{i,i}$, from the bound i-derived enolate (EN_i*) and a gaseous electrophile i) and to form a C−C bond with HCHO ($\Delta G^{TS}_{i,j}$, from the same bound EN_i* and a gaseous electrophile j):

$$\frac{k_{i,j}K_j}{k_{i,i}K_i} = \exp\left(-\frac{\Delta G^{TS}_{i,j-i,i}}{RT}\right) \quad (3)$$

$$\Delta G^{TS}_{i,j-i,i} = \Delta G^{TS}_{i,j} - \Delta G^{TS}_{i,i} \quad (4)$$

Measured $\frac{k_{i,j}K_j}{k_{i,i}K_i}$ ratios (1110 ± 40, Figure 4) correspond to $\Delta G^{TS}_{i,j-i,i}$ values of −45 ± 1 kJ mol^{-1} for acetone-HCHO reactions on TiO_2(a) at 773 K; these values are similar to the DFT-derived free energies reported below (Section 3.4).

3.4. Theoretical Treatments of Nucleophilic Attack at Carbonyl Compounds by Enolates on TiO_2 Surfaces.

DOI: 10.1021/jacs.7b11749
J. Am. Chem. Soc. 2018, 140, 775−782

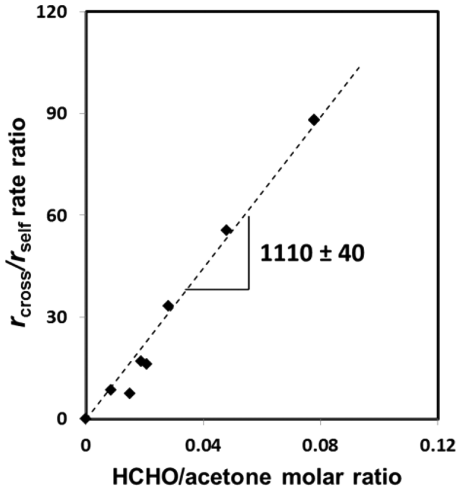

Figure 4. Effects of HCHO/acetone molar ratio on cross-condensation to self-condensation rate ratios (r_{cross}/r_{self}) for acetone-HCHO reactions (TiO_2(a); 20% wt. Ag/SiO_2; 1:8 mass ratio; 773 K, 0−10 kPa acetone, 0−10 kPa methanol, 10 kPa H_2, <5% acetone conversions; HCHO pressures measured in effluent stream). The dashed line represents a linear regression fit.

Scheme 4. Schematic Reaction Coordinate for C−C Coupling of Acetone-Derived Propen-2-olate with HCHO on Ti−O Site Pairs[a]

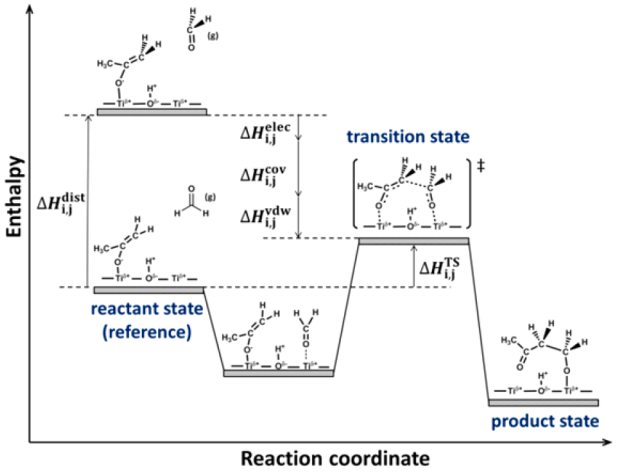

[a]The C−C coupling enthalpic barrier from propen-2-olate and HCHO(g) ($\Delta H_{i,j}^{TS}$) reflects the combined enthalpies of structural distortion of species in the reactant states to form the TS ($\Delta H_{i,j}^{dist}$) and of van der Waals ($\Delta H_{i,j}^{vdW}$), covalent ($\Delta H_{i,j}^{cov}$), and electrostatic ($\Delta H_{i,j}^{elec}$) interactions at the TS relative to their reactant states.

$Ti_5O_{19}H_{18}$ clusters were extracted from TiO_2(a) (101) surfaces (Scheme 2). Their five Ti atoms and the three internal O atoms were relaxed during geometry and energy optimizations (Section 2.3). The benchmarking of theory against measured rates of condensation and esterification[9,11] shows that $Ti_5O_{19}H_{18}$ clusters extracted from TiO_2(a) (101) surfaces (Scheme 2) provide adequate models for two-dimensional TiO_2(a) surfaces and for their ability to describe the confinement of bound species at two-dimensional rigid lattices; such models are used here to estimate $\Delta G_{i,j-i,i}^{TS}$ values for HCHO (j) and C_2−C_4 carbonyls (i) with enolates derived from the latter species. DFT-derived TS structures for C−C coupling between HCHO and enolates (Figure S2) resemble those for self-condensation of the carbonyl compounds,[9,11] but the C−C bond order (BO_{C-C}, a measure of the extent to which the C−C bond has formed)[35] at the TS is smaller for HCHO than for larger electrophiles for all the C_2−C_4 enolates examined (e.g., 0.29 and 0.37 for propen-2-olate couplings with HCHO and acetone, respectively; Table 1); such trends in bond orders are consistent with an earlier TS when HCHO acts as the electrophile. These trends in the location of the TS along the reaction coordinate reflect the stronger electrophilic character of the C atom in HCHO compared with the carbonyl C atom in the other reactants. Such trends in electrophilic character are consistent with the more exothermic nature of the reactions of F^- or CH_3^- anions with HCHO compared to those with the carbonyl C atoms in larger reactants (DFT-derived energies for the reactions of these anions with C_1−C_4 carbonyl molecules in gas phase shown in Table S2). Such reaction energies are essentially unaffected by steric effects for these carbonyl species because of the small sizes of the F^- and CH_3^- nucleophiles.

The effects of alkyl substituents on the enthalpy components ($\Delta H_{i,j}^{TS}$) of the activation free energy barriers for C−C coupling between gaseous carbonyl molecules and enolates bound at TiO_2(a) surfaces ($\Delta G_{i,j}^{TS}$) were examined first. Changes in $\Delta H_{i,j}^{TS}$, brought forth by steric and electronic effects of alkyl substituents in carbonyl reactants, have been proposed to determine relative reactivity and thus changes in the relative values of $\Delta G_{i,j}^{TS}$.[9,10] A Born−Haber thermochemical cycle (Scheme 4) is used to dissect $\Delta H_{i,j}^{TS}$ into enthalpy changes upon structural distortion of bound enolates and carbonyls in forming the TS ($\Delta H_{i,j}^{dist}$) and as they interact at the TS via van der Waals ($\Delta H_{i,j}^{vdW}$), covalent ($\Delta H_{i,j}^{cov}$), and electrostatic ($\Delta H_{i,j}^{elec}$) forces:

$$\Delta H_{i,j}^{TS} = \Delta H_{i,j}^{dist} + \Delta H_{i,j}^{vdW} + \Delta H_{i,j}^{cov} + \Delta H_{i,j}^{elec} \quad (5)$$

The $\Delta H_{i,j-i,i}^{TS}$ term in $\Delta G_{i,j-i,i}^{TS}$ (eq 4) can then be expressed as

$$\Delta H_{i,j-i,i}^{TS} = \Delta H_{i,j-i,i}^{dist} + \Delta H_{i,j-i,i}^{vdW} + \Delta H_{i,j-i,i}^{cov} + \Delta H_{i,j-i,i}^{elec} \quad (6)$$

where each $\Delta H_{i,j-i,i}^{X}$ term (X = dist, vdW, cov, or elec) is given by

$$\Delta H_{i,j-i,i}^{X} = \Delta H_{i,j}^{X} - \Delta H_{i,i}^{X} \quad (7)$$

$\Delta H_{i,j}^{dist}$ values depend weakly on temperature[29] and are approximated here by the corresponding electronic energies:

$$\Delta H_{i,j}^{dist} = E_{carbonyl}^{TS} - E_{carbonyl} + E_{EN}^{TS} - E_{EN} \quad (8)$$

Here $E_{carbonyl}^{TS}$ and E_{EN}^{TS} are the electronic energies for the bound carbonyl and enolate moieties at the TS, respectively, calculated separately for the gaseous carbonyl compound and the bound enolate using their respective structures at the TS, and $E_{carbonyl}$ and E_{EN} are those for the fully relaxed gaseous carbonyl compounds and the fully relaxed bound enolates as described in Section 2.3. $\Delta H_{i,j}^{elec}$ values were derived from classical Coulomb interactions that assume each atom in the TS structure is a point charge of a magnitude determined using the NBO analysis[34] (Section 2.3):

$$\Delta H_{i,j}^{elec} = \frac{1}{4\pi\varepsilon_0} \sum_{y=1}^{N} \sum_{x=1}^{M} \frac{C_x C_y}{r_{xy}} \quad (9)$$

where C_x and C_y represent the charge at the x atom in a bound carbonyl moiety with M C atoms and that at the y atom in a bound enolate with N C atoms, respectively, r_{xy} is the distance between the x and y atoms, and ε_0 is the permittivity of free space. Similar to the treatments used for $\Delta H_{i,j}^{elec}$, $\Delta H_{i,j}^{vdW}$ values

DOI: 10.1021/jacs.7b11749
J. Am. Chem. Soc. 2018, 140, 775−782

Table 1. DFT-Derived C−C Bond Orders (BO_{C-C}) at the TS, Activation Free Energies ($\Delta G^{TS}_{i,j-i,i}$) and Their Enthalpy ($\Delta H^{TS}_{i,j-i,i}$) and Entropy ($\Delta S^{TS}_{i,j-i,i}$) Components, and $k_{i,j}K_j/k_{i,i}K_i$ Ratios for Condensations of HCHO-C_{2-4} Carbonyl Mixtures with Different Enolates on Anatase TiO_2[a]

enolate reactant	carbonyl reactant	BO_{C-C}	$\Delta H^{dist}_{i,j-i,j}$ (kJ mol^{-1})[b]	$\Delta H^{vdW}_{i,j-i,j}$ (kJ mol^{-1})[b]	$\Delta H^{cov}_{i,j-i,j}$ (kJ mol^{-1})[b]	$\Delta H^{elec}_{i,j-i,j}$ (kJ mol^{-1})[b]	$\Delta H^{TS}_{i,j-i,i}$ (kJ mol^{-1})	$\Delta S^{ads}_{i,j-i,i}$ (J mol^{-1} K^{-1})[c]	$\Delta S^{TS}_{i,j-i,i}$ (J mol^{-1} K^{-1})	$\Delta G^{TS}_{i,j-i,i}$ (kJ mol^{-1})	$k_{i,j}K_j/k_{i,i}K_i$
ethenolate	ethanal	0.39	−43	9	24	2	−9	13	12	−18	16
	HCHO	0.33									
propen-1-olate	propanal	0.42	−72	18	48	−2	−8	20	20	−24	40
	HCHO	0.33									
buten-1-olate	butanal	0.41	−65	19	40	−1	−8	19	18	−21	28
	HCHO	0.32									
propen-2-olate	acetone	0.37	−69	15	45	6	−3	28	51	−43	784
	HCHO	0.29									
but-1-en-2-olate	butanone	0.37	−81	28	36	7	−10	32	44	−44	906
	HCHO	0.29									
but-2-en-2-olate	butanone	0.41	−115	37	51	14	−14	30	53	−55	4929
	HCHO	0.28									

[a] $Ti_5O_{19}H_{18}$ clusters, B3LYP+D3BJ, 6-311G(d,p) for C, H, and O atoms, LANL2DZ for Ti atoms; 773 K, 1 bar, optimized TS structures in Figure S2. [b] $\Delta H^{dist}_{i,j-i,j}$, $\Delta H^{vdW}_{i,j-i,j}$, $\Delta H^{cov}_{i,j-i,i}$ and $\Delta H^{elec}_{i,j-i,i}$ are the components of $\Delta H^{TS}_{i,j-i,i}$ from structural distortion and from van der Waals, covalent, and electrostatic interactions of the bound enolate and carbonyl moieties at the C−C coupling TS relative to their reactant states (eq 6). [c] The difference in entropy changes between gaseous i and j species upon their adsorption at a Ti center on TiO_2(a) surfaces (eq 10).

were determined using the two-body interaction potentials implemented in the D3BJ functionals.[26] $\Delta H^{cov}_{i,j}$ values were given by the difference between $\Delta H^{TS}_{i,j}$ and the sum of $\Delta H^{dist}_{i,j}$, $\Delta H^{elec}_{i,j}$, and $\Delta H^{vdW}_{i,j}$ (eq 5). These DFT-derived individual $\Delta H^{X}_{i,j}$ values (X = TS, dist, vdW, cov, or elec) for condensations of HCHO-C_{2-4} carbonyl mixtures on TiO_2(a) are included in Table S3 and used here to calculate $\Delta H^{X}_{i,j-i,i}$ values (eq 7) for each i−j carbonyl reactant pair, as described next.

Table 1 shows DFT-derived $\Delta H^{X}_{i,j-i,i}$ values for HCHO (j) and C_2−C_4 carbonyls (i) on TiO_2(a). $\Delta H^{dist}_{i,j-i,i}$ values are negative for all HCHO-(i) pairs (−43 to −115 kJ mol^{-1}) and become more negative as the number of C atoms in the molecule i increases. Such trends reflect the greater distortion required to form the C−C coupling TS for larger carbonyl nucleophiles in order to minimize steric effects upon interaction with a given enolate. $\Delta H^{vdW}_{i,j-i,i}$ values are positive (+9 to +37 kJ mol^{-1}), however, because larger carbonyls establish more effective van der Waals contacts with a given enolate. Covalent bonding at the TS is also weaker for HCHO than for larger carbonyls ($\Delta H^{cov}_{i,j-i,i}$: + 24 to +51 kJ mol^{-1}) for each enolate, even though HCHO is a stronger electrophile. This reflects the weaker σ−π^* orbital overlap at a C−C coupling TS structure that occurs significantly earlier along the reaction coordinate for the HCHO-enolate coupling pairs than for C−C coupling of enolates with larger carbonyl molecules. Such differences in σ−π^* orbital overlap are evident from their different C−C bond order at the TS (BO_{C-C}, Table 1), which correlates linearly with the corresponding $\Delta H^{cov}_{i,j-i,i}$ value for each reactant pair (Figure S3).

Electrostatic interactions between the enolate and the carbonyl co-reactant depend weakly on the electrophile ($\Delta H^{elec}_{i,j-i,i}$: −2 to 14 kJ mol^{-1}, Table 1), in contrast with van der Waals and covalent interactions ($\Delta H^{vdW}_{i,j-i,i}$ and $\Delta H^{cov}_{i,j-i,i}$), because carbonyl moieties are nearly neutral at the TS (Table S3). The overall $\Delta H^{TS}_{i,j-i,i}$ values resulting from the combined effects of distortion and of covalent, electrostatic, and van der Waals interactions vary only slightly (from −3 to −14 kJ mol^{-1}) for these i−j reactant pairs (Table 1), showing that the steric repulsion inherent in forming C−C coupling TS is almost fully compensated by stronger van der Waals and covalent interactions of enolates with the larger carbonyls. As a consequence, the enthalpic components in $\Delta G^{TS}_{i,j-i,i}$, typically associated with sterics and electrophilicity, are, in fact, not responsible for the very high reactivity of HCHO in nucleophilic attack by enolates at Lewis acid−base pairs on oxide surfaces.

These weak effects of alkyl substituents on $\Delta H^{TS}_{i,j}$ shown above render the entropy component ($\Delta S^{TS}_{i,j}$) in $\Delta G^{TS}_{i,j}$ critical in determining the relative values of $\Delta G^{TS}_{i,j}$ for each i−j carbonyl reactant pair at temperatures relevant for catalysis. DFT-derived $\Delta S^{TS}_{i,j-i,i}$ values for HCHO-C_{2-4} condensation vary between +12 and +53 J mol^{-1} K^{-1} (Table 1), indicating that activation entropies are less negative when HCHO acts as the electrophile and that they become increasingly negative for larger electrophiles (C_2−C_4 carbonyls). $\Delta S^{TS}_{i,j-i,i}$ values for C−C coupling with enolates derived from alkanals are nearly identical to the difference in entropies for species i and j (HCHO) upon their respective adsorption at a Ti center in the absence of any co-adsorbed species ($\Delta S^{ads}_{i,j-i,i}$, Table 1):

$$\Delta S^{ads}_{i,j-i,i} = S_{i^*} - S_{j^*} - S_{i(g)} + S_{j(g)} \quad (10)$$

where S_{i^*} and S_{j^*} are the entropies for bound i and j, respectively, and $S_{i(g)}$ and $S_{j(g)}$ are those for their gaseous precursors. The $\Delta S^{TS}_{i,j-i,i}$ values for alkanone-derived enolates are much larger than their $\Delta S^{ads}_{i,j-i,i}$ components (e.g., +28 and +51 J mol^{-1} K^{-1} for the respective $\Delta S^{ads}_{i,j-i,i}$ and $\Delta S^{TS}_{i,j-i,i}$ values of acetone-derived propen-2-olate, Table 1), because of rotational modes that become increasingly hindered as larger alkanones interact with the enolate at the C−C coupling TS.

These negative $\Delta H^{TS}_{i,j-i,i}$ values and positive $\Delta S^{TS}_{i,j-i,i}$ values for reactions of HCHO and C_2−C_4 alkanals/alkanones with a given enolate lead to negative $\Delta G^{TS}_{i,j-i,i}$ values at all relevant catalytic temperatures. For instance, the $\Delta G^{TS}_{i,j-i,i}$ value for HCHO-acetone reactants is −43 kJ mol^{-1} (773 K; Table 1) corresponding to $k_{i,j}K_j/k_{i,i}K_i$ ratios of about 800, in essential agreement with measurements (1110 ± 40, Figure 4). The kinetic preference for HCHO (as the electrophile) becomes stronger as temperature increases (Figure 5), because entropy benefits, brought forth by the strong effects of the size and structure of the carbonyl reactants on $\Delta S^{TS}_{i,j-i,i}$, become more consequential for the magnitude of the activation free energies at higher temperatures.

DOI: 10.1021/jacs.7b11749
J. Am. Chem. Soc. 2018, 140, 775−782

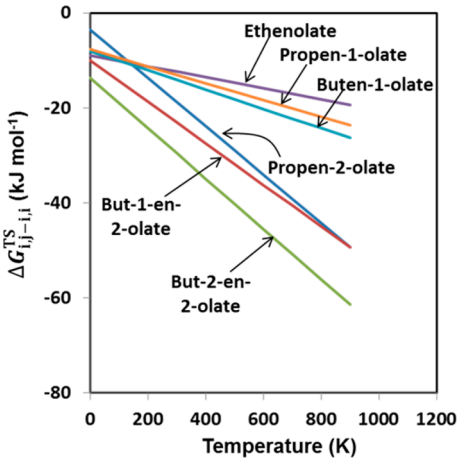

Figure 5. DFT-derived $\Delta G^{TS}_{i,j-i,i}$ as a function of temperature for condensations of HCHO-C_{2-4} carbonyl mixtures on anatase TiO_2.

The higher reactivity with HCHO is evident for all enolates, but the kinetic preference for HCHO becomes stronger for larger enolates, as shown by $\Delta G^{TS}_{i,j-i,i}$ values that become more negative as the number of C atoms or the extent of substitution in the enolates increases (Figure 5). These trends predominantly reflect the lower activation entropies when HCHO is the electrophile instead of enthalpic effects associated with steric repulsion or electrophilicity, which are balanced by van der Waals and covalent interactions for the larger electrophiles. Such entropy-driven high reactivity is unique for very small electrophiles, such as HCHO, because enthalpic effects prevail in determining the relative reactivities of C_{2+} carbonyl reactants in their nucleophilic attack by a given enolate on TiO_2(a) surfaces.[9]

These entropy-driven kinetic preferences for smaller and stronger electrophiles in C−C coupling with enolates on oxide surfaces differ from those attributed to weaker repulsive effects and to the low LUMO energies in HCHO in the case of condensation reactions in gaseous or liquid media.[10] The preeminence of entropy effects on surfaces reflects the greater extent of "organization" at the TS compared with processes occurring within less restrictive fluid media. The formation of such an "organized" TS imposes entropic penalties in exchange for enthalpic stabilization via covalent, electrostatic, and van der Waals interactions. These entropic penalties are least consequential for the smaller electrophiles when such reactions are mediated by the more organized TS made possible by the directing presence of a catalytic surface. Such consequences become most relevant at the high temperatures typical of condensation reactions on heterogeneous catalysts.

4. CONCLUSIONS

Bifunctional mixtures of anatase TiO_2 and Ag/SiO_2 are used to show the unique reactivity of HCHO (derived in situ from CH_3OH) in cross-condensations with enolates derived from larger carbonyl molecules. The latter co-reactants form enolates by kinetically relevant cleavage of their α-C−H bonds at Ti−O acid−base pairs on TiO_2 surfaces that remain essentially bare during catalysis. The preference for HCHO over large carbonyls as electrophiles in nucleophilic attack by a given enolate reflects a lower activation free energy barrier for the C−C coupling step on TiO_2 surfaces, evidenced from both experiments and theoretical treatments that account for van der Waals forces. DFT treatments also show that the more electrophilic nature of HCHO compared with larger carbonyl molecules leads to earlier TS for C−C coupling of bound enolates with HCHO, making the stability of these TS benefit less from the corresponding stronger C−C bond ultimately formed in the products compared with those for larger carbonyl reactants. The enthalpic contribution to the stability of such C−C coupling TS, however, is essentially unaffected by the size or electrophilicity of the carbonyl reactants, because the easier steric access and stronger electrophilic character of the carbonyl C atom in smaller reactants are compensated by their weaker van der Waals and covalent interactions with the enolate moiety at TS. Consequently, the relative free energy barriers for the C−C coupling of enolates with different carbonyl molecules are determined by the entropic losses upon formation of the bound TS from their gaseous reactant states. These findings elucidate the preeminent role of entropy underpinning the much higher reactivity of HCHO than larger carbonyl molecules in the nucleophilic attack by enolates on oxide surfaces at catalytically relevant temperatures.

■ ASSOCIATED CONTENT

Supporting Information

The Supporting Information is available free of charge on the ACS Publications website at DOI: 10.1021/jacs.7b11749.

Selectivity of methanol decomposition on Cu/SiO_2; derivation of condensation rate equations; DFT-derived structures for reactants, products, and TS of C−C coupling reactions; DFT-derived frequencies for vibrational modes of carbonyl molecules adsorbed on TiO_2; descriptors for the electrophilicity of carbonyl compounds; DFT-derived charges and activation enthalpies and entropies for C−C coupling TS; descriptors for the covalent interactions at C−C coupling TS (PDF)

■ AUTHOR INFORMATION

Corresponding Authors

*shuaiwang@xmu.edu.cn
*iglesia@berkeley.edu

ORCID

Enrique Iglesia: 0000-0003-4109-1001

Notes

The authors declare no competing financial interest.

■ ACKNOWLEDGMENTS

The authors acknowledge the financial support from BP p.l.c. through the XC^2 program and the computational resources provided by XSEDE and supported by the National Science Foundation (grant ACI-1548562). The authors are also grateful to Mr. Trenton Otto and Mr. Ari Fischer (University of California, Berkeley) for their careful proofreading and useful comments about the contents of this manuscript.

■ REFERENCES

(1) Carlini, C.; Flego, C.; Marchionna, M.; Noviello, M.; Galletti, A. M. R.; Sbrana, G.; Basile, F.; Vaccari, A. *J. Mol. Catal. A: Chem.* **2004**, *220*, 215−220.

(2) Carlini, C.; Marchionna, M.; Noviello, M.; Galletti, A. M. R.; Sbrana, G.; Basile, F.; Vaccari, A. *J. Mol. Catal. A: Chem.* **2005**, *232*, 13−20.

(3) Tanner, R.; Gill, P.; Wells, R.; Bailie, J. E.; Kelly, G.; Jackson, S. D.; Hutchings, G. J. *Phys. Chem. Chem. Phys.* **2002**, *4*, 688−695.

DOI: 10.1021/jacs.7b11749
J. Am. Chem. Soc. 2018, 140, 775−782

(4) Barrett, C. J.; Chheda, J. N.; Huber, G. W.; Dumesic, J. A. *Appl. Catal., B* **2006**, *66*, 111−118.
(5) Ivanova, I.; Sushkevich, V. L.; Kolyagin, Y.; Ordomsky, G. V. V. *Angew. Chem., Int. Ed.* **2013**, *52*, 12961−12964.
(6) Liu, Y.; Mfller, S.; Berger, D.; Jelic, J.; Reuter, K.; Tonigold, M.; Sanchez-Sanchez, M.; Lercher, J. A. *Angew. Chem., Int. Ed.* **2016**, *55*, 5723−5726.
(7) Okachi, T.; Onaka, M. *J. Am. Chem. Soc.* **2004**, *126*, 2306−2307.
(8) Van de Vyver, S.; Odermatt, C.; Romero, K.; Prasomsri, T.; Román-Leshkov, Y. *ACS Catal.* **2015**, *5*, 972−977.
(9) Wang, S.; Iglesia, E. *J. Phys. Chem. C* **2016**, *120*, 21589−21616.
(10) Yamataka, H.; Nagase, S.; Ando, T.; Hanafusa, T. *J. Am. Chem. Soc.* **1986**, *108*, 601−606.
(11) Wang, S.; Goulas, K.; Iglesia, E. *J. Catal.* **2016**, *340*, 302−320.
(12) Sun, J.; Zhu, K.; Gao, F.; Wang, C.; Liu, J.; Peden, C. H. F.; Wang, Y. *J. Am. Chem. Soc.* **2011**, *133*, 11096−11099.
(13) Sun, J.; Baylon, R. A. L.; Liu, C.; Mei, D.; Martin, K. J.; Venkitasubramanian, P.; Wang, Y. *J. Am. Chem. Soc.* **2016**, *138*, 507−517.
(14) An, W. *Phys. Chem. Chem. Phys.* **2015**, *17*, 22529−22532.
(15) Herrmann, S.; Iglesia, E. *J. Catal.* **2017**, *346*, 134−153.
(16) Gines, M. J. L.; Iglesia, E. *J. Catal.* **1998**, *176*, 155−172.
(17) Ren, L.; Dai, W.; Cao, Y.; Li, H.; Fan, K. *Chem. Commun.* **2003**, 3030−3031.
(18) Wang, S.; Zhang, Y.; Liu, H. *Chem. - Asian J.* **2010**, *5*, 1100−1111.
(19) Li, X.; Frisch, M. J. *J. Chem. Theory Comput.* **2006**, *2*, 835−39.
(20) Frisch, M. J.; Trucks, G. W.; Schlegel, H. B.; Scuseria, G. E.; Robb, M. A.; Cheeseman, J. R.; Scalmani, G.; Barone, V.; Mennucci, B.; Petersson, G. A.; Nakatsuji, H.; Caricato, M.; Li, X.; Hratchian, H. P.; Izmaylov, A. F.; Bloino, J.; Zheng, G.; Sonnenberg, J. L.; Hada, M.; Ehara, M.; Toyota, K.; Fukuda, R.; Hasegawa, J.; Ishida, M.; Nakajima, T.; Honda, Y.; Kitao, O.; Nakai, H.; Vreven, T.; Montgomery, J. A., Jr.; Peralta, J. E.; Ogliaro, F.; Bearpark, M.; Heyd, J. J.; Brothers, E.; Kudin, K. N.; Staroverov, V. N.; Kobayashi, R.; Normand, J.; Raghavachari, K.; Rendell, A.; Burant, J. C.; Iyengar, S. S.; Tomasi, J.; Cossi, M.; Rega, N.; Millam, M. J.; Klene, M.; Knox, J. E.; Cross, J. B.; Bakken, V.; Adamo, C.; Jaramillo, J.; Gomperts, R.; Stratmann, R. E.; Yazyev, O.; Austin, A. J.; Cammi, R.; Pomelli, C.; Ochterski, J. W.; Martin, R. L.; Morokuma, K.; Zakrzewski, V. G.; Voth, G. A.; Salvador, P.; Dannenberg, J. J.; Dapprich, S.; Daniels, A. D.; Farkas, Ö.; Foresman, J. B.; Ortiz, J. V.; Cioslowski, J.; Fox, D. J. *Gaussian 09*, Revision D.01; Gaussian, Inc.: Wallingford, CT, 2009.
(21) Becke, A. D. *J. Chem. Phys.* **1993**, *98*, 5648−5652.
(22) Lee, C.; Yang, W.; Parr, R. G. *Phys. Rev. B: Condens. Matter Mater. Phys.* **1988**, *37*, 785−789.
(23) McLean, A. D.; Chandler, G. S. *J. Chem. Phys.* **1980**, *72*, 5639−5648.
(24) Krishnan, R.; Binkley, J. S.; Seeger, R.; Pople, J. A. *J. Chem. Phys.* **1980**, *72*, 650−654.
(25) Hay, P. J.; Wadt, W. R. *J. Chem. Phys.* **1985**, *82*, 270−283.
(26) Grimme, S.; Ehrlich, S.; Goerigk, L. *J. Comput. Chem.* **2011**, *32*, 1456−1465.
(27) Boys, S. F.; Bernardi, F. *Mol. Phys.* **1970**, *19*, 553−566.
(28) Simon, S.; Duran, M.; Dannenberg, J. J. *J. Chem. Phys.* **1996**, *105*, 11024−11031.
(29) McQuarrie, D. A. *Statistical Mechanics*; University Science Books: Sausalito, CA, 2000.
(30) Merrick, J. P.; Moran, D.; Radom, L. *J. Phys. Chem. A* **2007**, *111*, 11683−11700.
(31) Grimme, S. *Chem. - Eur. J.* **2012**, *18*, 9955−9964.
(32) Hanna, D. G.; Shylesh, S.; Li, Y.-P.; Krishna, S.; Head-Gordon, M.; Bell, A. T. *ACS Catal.* **2014**, *4*, 2908−2916.
(33) Ayala, P. Y.; Schlegel, H. B. *J. Chem. Phys.* **1998**, *108*, 2314−2325.
(34) Martin, R. L. *J. Chem. Phys.* **2003**, *118*, 4775−4777.
(35) Wiberg, K. A. *Tetrahedron* **1968**, *24*, 1083−1096.
(36) Mayer, I. *J. Comput. Chem.* **2007**, *28*, 204−221.

DOI: 10.1021/jacs.7b11749
J. Am. Chem. Soc. 2018, 140, 775−782